Mem. S.A.It. Vol. 94, 80

**Memorie** della


# A multifaceted overlook of the galactic Halo through RR Lyrae

V. F. Braga[1,2], G. Bono[3], M. Fabrizio[2,4], J. Crestani[3], S. Kwak[3], M. Dall'Ora[5], V. D'Orazi[2], G. Fiorentino[2], M. Marengo[6], S. Marinoni[2,4], P. M. Marrese[2,4], and M. Monelli[1]

[1] IAC Instituto de Astrofísica de Canarias, Calle Vía Láctea sn, 38201 La Laguna, Tenerife, Spain
[2] Istituto Nazionale di Astrofisica – Osservatorio Astronomico di Roma, via Frascati 33, Monte Porzio Catone, 00078, Italy
[3] Universitá di Tor Vergata – Dipartimento di Fisica, via della Ricerca Scientifica 1, Roma, 00133, Italy
[4] ASI – Space Science Data Center, via del Politecnico, Roma, 00133, Italy
[5] Istituto Nazionale di Astrofisica – Osservatorio Astronomico di Capodimonte, salita Moiariello 16, Napoli, 80131, Italy
e-mail: vittorio.braga@inaf.it
The remaining affiliations can be found at the end of the paper.

Received: 19 December 2022; Accepted: 28 December 2022

**Abstract.** We have built the largest dataset of RR Lyrae stars (286,175 RRLs) by joining public catalogs cross-matched with Gaia DR2 and DR3. We also collected and homogeneously reduced public/proprietary spectra of 9,299 RRLs. We used the DR2 version of this catalog as the starting point for several investigations of the oldest part of the Milky Way. We found an [Fe/H] distribution peaked at ∼–1.5 and extended from ∼–3 to supersolar. Our data show evidence of a P-[Fe/H] relation and, based on this, we argue that the long-standing problem of the Oosterhoff dichothomy is due to the lack of intermediate-metallicity Globular Clusters with a sizeable sample of RRLs. We provide the first [$\alpha$/Fe]-[Fe/H] diagram for purely old stars, where RRLs do not show the typical bimodal behavior of Halo stars of all ages, thus indicating that the dichothomy could be an age effect. Finally, we provide Radial Velocity (RV) curve templates, that can be adopted to measure the systemic velocities of RRLs with only a few RV measurements.

**Key words.** Stars: Variables: RR Lyrae stars – Galactic Halo

## 1. Introduction

In the last years, the entire field of Milky Way (MW) astronomy has seen significant improvements thanks to the synergy between Gaia (Gaia Collaboration et al. 2018) and data from large spectroscopic surveys (APOGEE, LAMOST, GALAH, to name the largest). While Gaia provides the 5-D astrometry (celestial coordinates, proper motions and parallaxes) of ∼1% of the stars in the MW, the spectroscopic data add the $6^{th}$ dimension (the ra-

dial velocity, RV) and chemical abundances for millions of stars.

These data allowed the detection of several mergers (Belokurov et al. 2018; Naidu et al. 2020) and tens of streams in the Halo (Helmi 2020), validating the hierarchical assembly model of the MW (Searle & Zinn 1978). For all these investigations, the Halo is the most important component of the MW. In fact, the Halo is mainly old and the relaxation times of stellar orbits are of the order of $10^{12}$ yr (Woolley & Stewart 1967). This means that its stars keep the information of the primordial ages and can be used as fossil records of the MW formation.

RR Lyrae variables (RRLs) are low-mass, core-Helium burning stars on the Horizontal Branch (HB), meaning that they are strictly old ($\gtrsim$10 Gyr, Cox 1974). RRLs are also well-known standard candles that obey tight Period-Luminosity relations (PLRs) in the Near- and Mid-Infrered (NIR, MIR) bands, (Longmore et al. 1986; Madore et al. 2013), allowing accurate individual distance measurements (~2-5% uncertainty in the inner Halo and ~10% within 200 kpc). Finally, their pulsation properties are also affected by their metallicity, with a clear Period-[Fe/H] relation (Sandage 1982; Fabrizio et al. 2019). These characteristics make them optimal tracers of the structure and evolution of the old component of the MW and, more specifically, of the Halo.

In this contribute, we present the largest catalog of MW RRLs, with a specific focus on the Halo. This catalog will be the starting point for any investigation of the MW formation using RRLs as stellar tracer. In §2, we describe the catalog, its properties and how we assembled it. In §3, we discuss the results obtained by exploiting the catalog. In §4 we provide a summary and discuss the future developments.

## 2. The catalog

We started to build the catalog with the aim of including full astrometric, photometric, spectroscopic and pulsation properties for the RRLs in the Halo. To achieve this result, four main data sets are needed: 1) Gaia data; 2) Photometric data from variability surveys ; 3) All-sky NIR and MIR photometric data; 4) Spectroscopic data. In the following, we describe how we built the catalog starting from these data sets.

### 2.1. Photometric catalog

The Gaia mission has two main advantages that make its data the foundation of our catalog. Firstly, it is the most precise all-sky astrometry mission, and this will be true for at least one more decade; secondly, it is also a variability survey, because it provides time series in three bands with tens of phase points for hundreds of thousands of RRLs. Its tables also include the pulsation properties (periods, amplitudes, flux-averaged magnitudes to name the most important) of RRLs. Note that we started to build the catalog in 2018, having only Gaia DR2 available (Gaia Collaboration et al. 2018; Clementini et al. 2019). Lately, we have extended the catalog to Gaia DR3 (Gaia Collaboration et al. 2022; Clementini et al. 2022).

However, for our purpose, a standalone catalog of Gaia would not provide enough information. Therefore, we decided to complement the Gaia data with those from variability surveys like CATALINA, LINEAR, LONEOS-I, NSVS, ROTSE-I, QUEST-I, ASAS, ASAS-SN, DECAM, PanSTARRS, ZTF (Fabrizio et al. 2021, and references therein). Note that we did not include OGLE-IV (Udalski et al. 2015) among the variability surveys. The reason for this decision is twofold: 1) OGLE-IV observes the Bulge, Magellanic Clouds and Galactic Disk while, as already mentioned, we are mostly interested in the Halo; 2) To cross-match the Gaia catalog with external catalogs, we adopted the accurate cross-match algorithm by Marrese et al. (2019). However, the OGLE-IV survey focuses on very dense regions (the bulge, plane, Magellanic Clouds) and this algorithm is not optimal to map Gaia into this type of catalog.

There are several advantages when including these surveys to the Gaia catalog of RRLs. First of all, these surveys provide time series either in the $V$ band, which is the reference passband in the literature, or in the

*ugriz* system, which will be the photometric system of the future concerning variability, especially when LSST will start to deliver its data. Moreover, the time series of the quoted surveys have about a factor of ten more phase points than Gaia time series. This means that their periods are usually more accurate. Finally, by adding these surveys we could extend the catalog by ∼30% starting from the Gaia DR2 RRL catalog (5-10% starting from Gaia DR3), with objects that are not in Gaia's variability tables, but are in Gaia's main catalog (`gaiadr3.gaia_source`). We ended up with a catalog of 177,998/286,175 RRLs (DR2/DR3, see Figure 2.1).

Unfortunately despite being crucial for the geometrical calibration of the PLRs, Gaia parallaxes have uncertainties larger than 10% for RRLs farther than ∼6 kpc. This meas that, for the majority of the RRLs in the sample, Gaia parallaxes would not provide precise distances. For this reason, it is crucial to add NIR and MIR magnitudes to the catalog, in order to estimate distances by exploiting the PLRs of RRLs in these bands. Adopting the cross-match algorithm by Marrese et al. (2019), we included in our catalog the *ugrizJHKW1W2* properties of RRLs from the SDSS (Ahn et al. 2012), allWISE (Wright et al. 2010) and 2MASS (Skrutskie et al. 2006) point source catalogs.

## 2.2. Spectroscopic data

To complement the astrometric, positional, kinematical and pulsation properties of RRLs, we collected the largest spectroscopic dataset for RRLs. We ended up with 22,922 spectra for 9,299 RRLs. Note that this dataset includes both high- medium- and low-resolution (HR, MR, LR) spectra, from proprietary and public data, both from large surveys and small observation programmes.

### 2.2.1. Chemical abundances

We have reduced the HR spectra starting from a line list of of 415 Fe I and 56 Fe II lines, cleaned of blended lines using the Moore et al. (1966) solar spectrum atlas and synthetic spectra as a reference. We derived the effective temperature ($T_{eff}$), surface gravity ($\log g$) and metallicity [Fe/H] for each spectrum using the equivalent widths (EWs) of Fe I and Fe II. Once the properties of the atmosphere were optimized we derived, only for the HR spectra, the abundance of all elements (Fe, $\alpha$, neutron capture) by the EW of their absorption lines.

**Table 1.** Key properties of the different spectroscopic datasets adopted. Note that the totals of columns 2 and 3 take into account multiple occurrences in different datasets

| Instrument | $N_{spectra}$ | $N_{RRab}$ | $N_{RRc}$ |
|---|---|---|---|
| —High resolution— | | | |
| du Pont | 6200 | 112 | 76 |
| FEROS@2.2m | 55 | 3 | 0 |
| HARPS-N@TNG | 10 | 0 | 4 |
| HARPS@3.6m | 315 | 18 | 6 |
| HRS@SALT | 81 | 64 | 5 |
| SES@STELLA | 100 | 0 | 8 |
| HDS@Subaru | 34 | 23 | 2 |
| UVES@VLT | 277 | 62 | 8 |
| —Medium resolution— | | | |
| X-Shooter@VLT | 121 | 16 | 2 |
| LAMOST-MR | 936 | 90 | 55 |
| —Low resolution— | | | |
| LAMOST-LR | 8785 | 4162 | 1836 |
| SEGUE-SDSS | 6008 | 3154 | 1574 |
| —Total— | | | |
| | 22922 | 6863 | 3125 |

In principle, LR and MR spectra do not allow to estimate [Fe/H] from the EWs of Fe lines. However, one can adopt the so-called ΔS method (Preston 1959), that provides an estimate of [Fe/H] by comparing the EWs of the Ca II K, $H_\beta$, $H_\gamma$ and $H_\delta$ lines. We point out that RRLs are suitable stars to apply the ΔS method because one can assume that their $\log g$ are constant. Since $T_{eff}$ affects the EWs of Ca and Balmer lines with opposite signs, one can assume that the difference in EW, only depends on the metallicity (Gratton et al. 2004).

By degrading the HR spectra to low resolution ($R \approx 2000$), we provide a new calibration of the ΔS method for both RRab and RRc (Fabrizio et al. 2019; Crestani et al. 2021b). The [Fe/H] estimates obtained with this method are less precise than those obtained

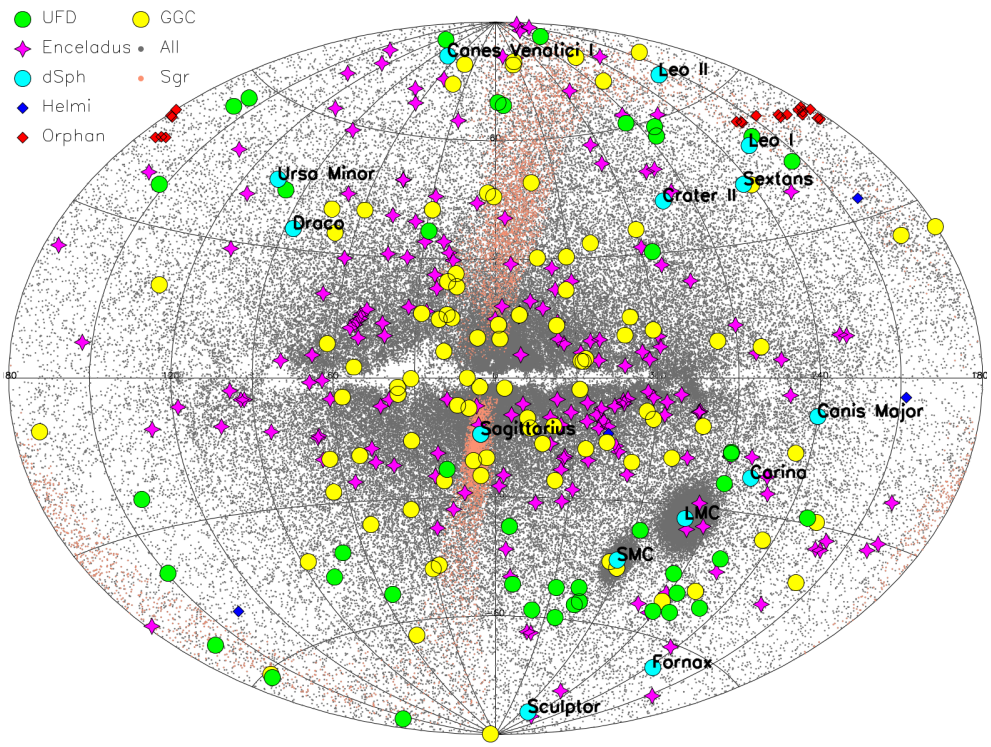


**Fig. 1.** Distribution in Galactic coordinates of the photometric dataset. Stellar systems or stellar streams hosting RRLs are marked with different symbols and/or colours (see labels).

with HR spectra (0.2-0.3 dex versus 0.10-0.15 dex) but since the largest spectroscopic surveys usually provide LR spectra, this means to increase by almost two orders of magnitude the RRLs with available [Fe/H] estimate.

### 2.2.2. Radial velocities

To derive RV measurements, we adopted multiple spectroscopic diagnostics: three lines of the Fe I multiplet 43, a resonant Sr II line, the Na doublet (D1 and D2), the Mg I b triplet (Mg $b_1$, Mg $b_2$ and Mg $b_3$), $H_\alpha$, $H_\beta$, $H_\gamma$ and $H_\delta$. We did not average the RVs from these different diagnostics but kept them in separated data sets. This decision was dictated by the fact that different lines form at different optical depths and, for pulsating stars like RRLs, trace the expansion/contraction of different layers. In fact, since RRLs are pulsating stars, any RV measurement of these objects consists of the sum of the systemic velocity of the barycenter ($V_\gamma$, constant) and of the pulsation velocity of the layer where the line forms ($V_P$, periodically variable). The median uncertainties of the single RV estimates are on average, smaller than 1.5 km/s.

We point out that we have RV measurements for all the almost 10,000 stars in the spectroscopic sample. Among hese, only 74 of them display a well-sampled pulsation cycle, but they are enough to build the RV curve templates (see Section 3.3)

## 3. Main results

The catalog that we have built is, since four years, our reference catalog for any study of Galactic RRLs, especially in the Halo. In the following, we will discuss the main results obtained. Note that, since the catalog was extended to Gaia DR3 only in the last months,

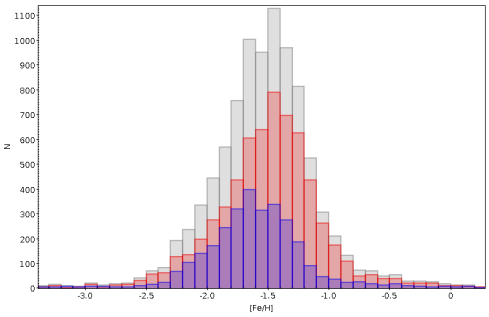


**Fig. 2.** [Fe/H] distribution of the RRLs of our catalog. Grey bars indicate all RRLs, red bars indicate RRab, blue bars indicate RRc.

all the presented results are based on our Gaia DR2-based catalog.

### *3.1. Metallicity distribution*

We have provided the metallicity distribution of RRLs in three different papers over time (Fabrizio et al. 2019; Crestani et al. 2021b; Fabrizio et al. 2021), with results that remained consistent each time the catalog was extended or the ΔS calibration was improved. More specifically, the [Fe/H] average is –1.51±0.01 dex, with a standard deviation of 0.41 dex (see Fig. 3.1). The tails, however, reach ∼–3 dex on one side and supersolar metallicities (∼+0.2) on the other.

The distribution is skewed towards the metal-poor regime: the number of stars at –2 dex is almost twice as that at –1 dex. This is an expected feature, due to the strictly old age of these stars, which favours, on average, metal-poor over metal-rich chemical composition. One can also note that the distributions of RRab and RRc peak at –1.48±0.01 dex and –1.58±0.01 dex, respectively. This is consistent with evolutionary models. In fact, the Horizontal Branch becomes systematically redder with increasing metallicity (Torelli et al. 2019), and RRc populate the bluest part of the Instability Strip (Cox et al. 1983). These two effects are telling us that RRc are more easily found in metal-poor environments, thus providing a justification for our finding.

Finally, we have validated empirically the P-[Fe/H] relation theorized by Sandage (1982), finding $\log P = -0.293 - 0.036 \times [Fe/H]$ and $\log P = -0.558 - 0.051 \times [Fe/H]$ for RRab and RRc, respectively (Fabrizio et al. 2019, 2021).

#### 3.1.1. Oosterhoff dichothomy

The Oosterhoff dichothomy is a long-standing open astrophysical issue: the Globular Clusters (GCs) of the MW are separated into two main different classes (Oosterhoff I and II) based on the mean period of their RRab ($< P_{ab} >$=0.55 and $< P_{ab} >$=0.65 days, respectively, Oosterhoff 1939). This dichothomy is clearly visible by a gap in a [Fe/H] vs $< P_{ab} >$ plane; on the other hand, dwarf spheroidals and the GCs of M31 display no gap (Catelan 2009).

The gap can be easily explained by considering together the P-[Fe/H] relation and the lack of metal-intermediate GCs with a sizeable sample of RRLs, from which the Oosterhoff dichothomy in the MW arises naturally.

### *3.2. α elements*

$\alpha$ elements are crucial when inspecting the properties of the birthplace of stars: they are ejected in the interstellar medium mostly by Supernovae (SNe) type II, that are the outcome of high-mass stars and happen on short evolutionary timescales. Iron, instead, is mostly ejected by SNe type Ia, associated to white dwarfs, on much slower timescales. Therefore, the [$\alpha$/Fe] ratio provides constraints on the dominating pollution processes at the time of formation of the target stars.

We have derived, from HR spectra, the abundances of Mg, Ca, Ti I and Ti II. Note that the abundance of Mg is usually based on a couple of lines, while those of Ca and Ti are based on 5-15 lines, thus leading to higher uncertainties in Mg abundances. By averaging the [Mg/Fe], [Ca/Fe] and [Ti/Fe], values, we obtained the [$\alpha$/Fe], plotted in Fig. 3.2. Crestani et al. (2021a) showed that the three elements display a similar behavior, the only difference being a larger dispersion, at [Fe/H]$\lesssim$–1.2, of [Mg/Fe]. The reasons contributing to this ef-

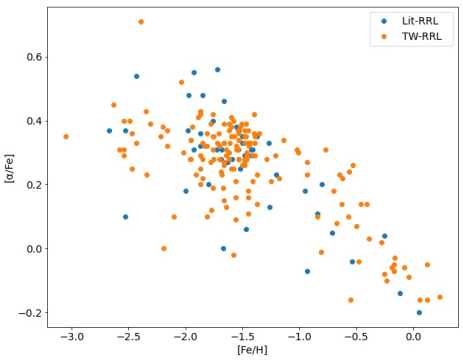


**Fig. 3.** [$\alpha$/Fe] vs [Fe/H] distribution for RRLs. Orange points mark RRLs for which we reduced the spectra, blue points mark literature data.

fect are two, one being a bias (the lower number of stars for Mg lines), the second indicating a real scatter in Mg, due to the dependence of the production of this element with stellar mass (McWilliam 1997).

Crestani et al. (2021a) also noted that the RRL distribution overlaps that of Sagittarius Red Giants (RGs), while Fornax RGs are less $\alpha$ enhanced by 0.3-0.4 dex, suggesting that dwarf galaxies of that size might have contributed mainly to the formation of the metal-rich Halo, but not to the metal-poor component.

Unlike [$\alpha$/Fe] vs [Fe/H] planes populated by stars of all ages, where the distribution is bimodal (e.g. Hayes et al. 2018; Gallart et al. 2019), RRLs are distributed within a single group of objects. We therefore suggest that the dichothomy observed in other works is, at least in part, an age effect.

### 3.3. Radial velocity curve template

As already mentioned in Section 2.2.2, stellar pulsations affect the RV measurements, because also the motion of the expanding/contracting layer contributes to the displacement of the absorption lines. In fact, the RV variations follow a cycle having the same period as the light variations. If one does not have enough RV measurements to cover the entire cycle, $V_\gamma$ cannot be estimated by integrating over the fit of the RV curve.

To collect spectroscopic time series is very costly concerning the telescope time, therefore, large spectroscopic surveys usually collect a small number of spectra for each target (usually less than five, except for calibration fields, depending on the observation strategy). This can lead to 40-70 km/s errors in the estimate of $V_\gamma$, depending on the diagnostic adopted (Balmer lines display RV-curves with decreasing amplitudes from $H_\alpha$ to $H_\delta$, and metallic lines have even smaller amplitudes than $H_\delta$ Bono et al. 2020).

RV curve templates can be adopted to accurately estimate $V_\gamma$, provided that the ephemerides and the $V$-band amplitude of the pulsation ($Amp(V)$) is known, even when only one RV measurement is available (Liu 1991; Sesar 2012). In Braga et al. (2021), we provided new RV-curve templates having several advantages with respect to the previous ones. 1) We provided templates of RRc for the first time; 2) The period range covered by our templates is 0.27-0.84 days, while those by Sesar (2012) covered only a very narrow range (0.56-0.59 days); 3) We provided, for the first time, the $H_\delta$ RV-curve templates and separate Fe, Mg and Na RV-curve templates, instead of a generic "metallic" one. 4) We have a number of RV measurements more than six times larger than those used previously.

When using the templates, if less than three RV measurements are available, the anchor epoch ($T_0$) is crucial. In the literature and in all the largest photometric surveys, the reference epoch provided for pulsating stars is the epoch of maximum light ($T_{max}$). Inno et al. (2015) started adopting, for Classical Cepheids (CCs), the time of the mean magnitude on the rising branch ($T^{ris}_{mean}$), arguing that it is more stable and avoids the problem of the flat/double maximum for CCs on the Hertzsprung progression. In Braga et al. (2021), we finally provide quantitative evidence that adopting $T^{ris}_{mean}$ instead of $T_{max}$ provides dispersions $\sim$30% smaller for cumulated light and radial velocity curves. Knowing, however, that $T_{max}$ is still

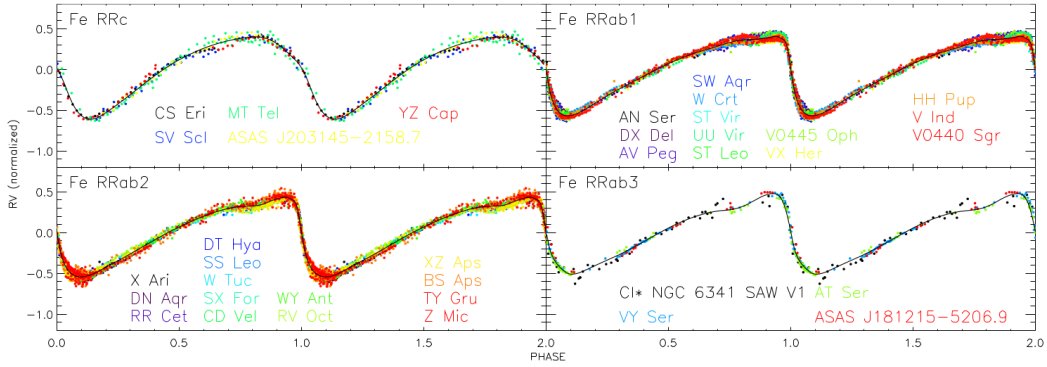


**Fig. 4.** Cumulated Fe RV curves in four period bins. The bin is labelled on the upper-left corner of each panel. Different RRLs in different bins are color-coded.

more popular, we also provided simple formulae to convert the phases obtained by anchoring at $T_{max}$ into phases anchored at $T^{ris}_{mean}$: $\Delta\phi$ = 0.043 + 0.099×P ($\sigma$=0.024) for RRab; $\Delta\phi$ = 0.223 ($\sigma$=0.036) for RRc.

## 4. Conclusions

We have built an astrometric-photometric-spectroscopic catalog of 286,175 RRLs based on Gaia DR3, and extended with independent RRL detections by other variability surveys. This is the largest catalog of MW RRLs, and includes also the largest number of RRLs with spectroscopic data (almost 10,000).

This catalog can be the starting point for any investigation of the RRLs in the MW, both as distance indicators, population tracers and Galactic Archaeology relics of the MW formation. We already obtained, from an earlier Gaia DR2 version of the catalog, important results concerning the metallicity distribution of the oldest component of the Halo, found an empirical validation of the P-[Fe/H] relation—which also naturally explains the Oosterhoff dichothomy—and provideed RV-curve templates of unprecedented completeness and precision.

We are currently at work to provide also the abundances of neutron-capture elements for a couple of hundreds of RRLs for which we have HR spectra. We also plan to geometrically calibrate the NIR PLR for ∼1,000 RRLs for which we have accurate Gaia DR3 parallaxes and to constrain the density profile and the metallicity gradient of the Halo as traced by RRLs.

In the future, the catalog will be extended, both in size and in the content of spectroscopic data. The first task will be achieved by including data from new photometric surveys (Gaia DR4, LSST) and will likely lead to a catalog with more than 500,000 RRLs. Large spectroscopic surveys of the future, especially WEAVE, 4MOST, MOONS, DESI and, later, MSE, will increase by at least a factor of two-three the number of RRLs with associated spectroscopic data. This will allow, in the next four-five years, to adopt RRLs as tracers of the MW formation.

**Affiliations**

[6] Department of Physics and Astronomy, Iowa State University, Ames, IA 50011, USA

*Acknowledgements.* V.F. Braga is grateful to the organizers for the invitation. V.F. Braga and M. Monelli acknowledge financial support from the ACIISI, Consejería de Economía, Conocimiento y Empleo del Gobierno de Canarias and the European Regional Development Fund (ERDF) under the grant with reference ProID2021010075.

## References

Belokurov, V., Deason, A. J., Koposov, S. E., et al. 2018, MNRAS, 477, 1472

Bono, G., Braga, V. F., Crestani, J., et al. 2020, ApJ, 896, L15

Braga, V. F., Crestani, J., Fabrizio, M., et al. 2021, ApJ, 919, 85
Catelan, M. 2009, Ap&SS, 320, 261
Clementini, G., Ripepi, V., Garofalo, A., et al. 2022, arXiv e-prints, arXiv:2206.06278
Clementini, G., Ripepi, V., Molinaro, R., et al. 2019, A&A, 622, A60
Cox, A. N., Hodson, S. W., & Clancy, S. P. 1983, ApJ, 266, 94
Cox, J. P. 1974, Reports on Progress in Physics, 37, 563
Crestani, J., Braga, V. F., Fabrizio, M., et al. 2021a, arXiv e-prints, arXiv:2104.08113
Crestani, J., Fabrizio, M., Braga, V. F., et al. 2021b, ApJ, 908, 20
Fabrizio, M., Bono, G., Braga, V. F., et al. 2019, ApJ, 882, 169
Fabrizio, M., Braga, V. F., Crestani, J., et al. 2021, ApJ, 919, 118
Gaia Collaboration, Brown, A. G. A., Vallenari, A., et al. 2018, A&A
Gaia Collaboration, Vallenari, A., Brown, A.G.A., Prusti, T., & et al. 2022, A&A
Gallart, C., Bernard, E. J., Brook, C. B., et al. 2019, Nature Astronomy, 3, 932
Gratton, R., Sneden, C., & Carretta, E. 2004, ARA&A, 42, 385
Hayes, C. R., Majewski, S. R., Shetrone, M., et al. 2018, ApJ, 852, 49
Helmi, A. 2020, arXiv e-prints, arXiv:2002.04340
Inno, L., Matsunaga, N., Romaniello, M., et al. 2015, A&A, 576, A30
Liu, T. 1991, PASP, 103, 205
Longmore, A. J., Fernley, J. A., & Jameson, R. F. 1986, MNRAS, 220, 279
Madore, B. F., Hoffman, D., Freedman, W. L., et al. 2013, ApJ, 776, 135
Marrese, P. M., Marinoni, S., Fabrizio, M., & Altavilla, G. 2019, A&A, 621, A144
McWilliam, A. 1997, ARA&A, 35, 503
Moore, C. E., Minnaert, M. G. J., & Houtgast, J. 1966, The solar spectrum 2935 A to 8770 A
Naidu, R. P., Conroy, C., Bonaca, A., et al. 2020, ApJ, 901, 48
Oosterhoff, P. T. 1939, The Observatory, 62, 104
Preston, G. W. 1959, ApJ, 130, 507
Sandage, A. 1982, ApJ, 252, 553
Searle, L. & Zinn, R. 1978, ApJ, 225, 357
Sesar, B. 2012, AJ, 144, 114
Skrutskie, M. F., Cutri, R. M., Stiening, R., et al. 2006, AJ, 131, 1163
Torelli, M., Iannicola, G., Stetson, P. B., et al. 2019, A&A, 629, A53
Udalski, A., Szymański, M. K., & Szymański, G. 2015, ActaA, 65, 1
Woolley, Richard, S. & Stewart, J. M. 1967, MNRAS, 136, 329
Wright, E. L., Eisenhardt, P. R. M., Mainzer, A. K., et al. 2010, AJ, 140, 1868